



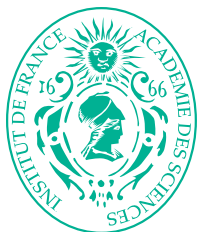
## The core structure of screw dislocations with [001] Burgers vector in $\text{Mg}_2\text{SiO}_4$ olivine

Downloaded from: <https://research.chalmers.se>, 2025-12-04 22:41 UTC

Citation for the original published paper (version of record):

Mahendran, S., Carrez, P., Cordier, P. (2021). The core structure of screw dislocations with [001] Burgers vector in  $\text{Mg}_2\text{SiO}_4$  olivine. *Comptes Rendus Physique*, 22(S3).  
<http://dx.doi.org/10.5802/CRPHYS.27>

N.B. When citing this work, cite the original published paper.



INSTITUT DE FRANCE  
Académie des sciences

# *Comptes Rendus*

---

## *Physique*

Srinivasan Mahendran, Philippe Carrez and Patrick Cordier

**The core structure of screw dislocations with [001] Burgers vector in  $\text{Mg}_2\text{SiO}_4$  olivine**


Online first (2021)

<<https://doi.org/10.5802/crphys.27>>

**Part of the Special Issue:** Plasticity and Solid State Physics

**Guest editors:** Samuel Forest (Mines ParisTech, Université PSL, CNRS, France)  
and David Rodney (Université Claude Bernard Lyon 1, France)

© Académie des sciences, Paris and the authors, 2021.  
*Some rights reserved.*

 This article is licensed under the  
CREATIVE COMMONS ATTRIBUTION 4.0 INTERNATIONAL LICENSE.  
<http://creativecommons.org/licenses/by/4.0/>



*Les Comptes Rendus. Physique sont membres du  
Centre Mersenne pour l'édition scientifique ouverte*  
[www.centre-mersenne.org](http://www.centre-mersenne.org)



# The core structure of screw dislocations with [001] Burgers vector in $\text{Mg}_2\text{SiO}_4$ olivine

## *Structure de coeur de la dislocation vis de vecteur de Burgers [001] dans l'olivine $\text{Mg}_2\text{SiO}_4$*

Srinivasan Mahendran<sup>a, b</sup>, Philippe Carrez<sup>\*, a</sup> and Patrick Cordier<sup>a, c</sup>

<sup>a</sup> Univ. Lille, CNRS, INRAE, Centrale Lille, UMR 8207 – UMET – Unité Matériaux et Transformations, F-59000 Lille, France

<sup>b</sup> Department of Physics, Chalmers University of Technology, Gothenburg 412 96, Sweden

<sup>c</sup> Institut Universitaire de France, 1 rue Descartes, F-75005 Paris, France

E-mails: [srinivasan.mahendran@gmail.com](mailto:srinivasan.mahendran@gmail.com) (S. Mahendran),  
[philippe.carrez@univ-lille.fr](mailto:philippe.carrez@univ-lille.fr) (P. Carrez), [patrick.cordier@univ-lille.fr](mailto:patrick.cordier@univ-lille.fr) (P. Cordier)

**Abstract.** In this study, we report atomistic calculations of the core structure of screw dislocations with [001] Burgers vector in  $\text{Mg}_2\text{SiO}_4$  olivine. Computations based on the THB1 empirical potential set for olivine show that the stable core configurations of the screw dislocations correspond to a dissociation in {110} planes involving collinear partial dislocations. As a consequence, glide appears to be favorable in {110} planes at low temperature. This study also highlights the difference between dislocation glide mechanism in {110} versus (010) or (100) for which glide is expected to occur through a locking–unlocking mechanism.

**Résumé.** Dans cette étude, nous présentons les résultats de calculs atomiques de la structure de coeur de la dislocation vis de vecteur de Burgers [001] dans l'olivine  $(\text{Mg,Fe})_2\text{SiO}_4$ . Nos simulations, reposant sur l'utilisation du potentiel semi-empirique THB1, montrent que la configuration stable de la dislocation vis correspond à une structure de coeur dissociée dans les plans {110}. A basse température, le glissement des dislocations de vecteur de Burgers [001] dans les plans {110} de l'olivine est donc favorisé.

**Keywords.** Atomistic simulations, Crystal plasticity, Dislocation glide, Core structure, Olivine.

**Mots-clés.** Simulations à l'échelle atomique, Plasticité, Dislocation, Structure de coeur, Glissement, Olivine.

---

\* Corresponding author.

## 1. Introduction

Since the work of Peierls and his seminal paper entitled “The size of a dislocation” [1], it has been well established that the exact atomic arrangement in the vicinity of the dislocation core is a key issue in plasticity. Besides the elastic properties of the defect, most intrinsic properties of dislocations are directly related to the core structure [2]. Among these properties, are the lattice friction opposed by the crystal to the dislocation motion [3–6], the ability to glide or cross-slip in different planes [7–10], the extension of kinks with or without friction [11–13] or the jogs configurations and planes [14–16]. It is worth noticing that previously mentioned intrinsic properties also apply to more complex materials than simple metals, including, L12 alloys [17], oxides [18, 19], ceramics or minerals [20–23].

Because of their importance to understand the nature of deformations in the Earth interior, the plastic properties of some minerals have been extensively studied. Among those, one of the most studied minerals is olivine, a silicate of chemical composition  $(\text{Mg,Fe})_2\text{SiO}_4$ , which is a major component of the Earth upper mantle down to 410 km depth. Olivine is orthorhombic (*Pbnm* space group) and at ambient pressure and temperature, the lattice constants are  $a = 4.756 \text{ \AA}$ ,  $b = 10.207 \text{ \AA}$  and  $c = 5.98 \text{ \AA}$  [24]. It is now commonly accepted that  $[010]$  glide is not activated in olivine and that the plastic properties result from activation of two types of dislocations with  $[100]$  and  $[001]$  Burgers vectors, the two shortest lattice repeats of the lattice [25]. This results not only from laboratory experiments [26–29], but also from observations of natural samples made with optical microscopy or Transmission Electron Microscopy (TEM) techniques [30]. Using deformation experiments performed at ambient pressure on polycrystalline olivine, Raleigh [26] showed that the deformation of olivine results from the activation of  $[001]$  glide at low temperature and relatively high-stress conditions, whereas above  $1000 \text{ }^\circ\text{C}$ , Carter and Ave'Lallemant [31] observed activation of  $[100]$  slip. Deformation experiments performed on single crystals lead to the same conclusion but also gave access to quantitative information on the mechanical behavior of individual slip systems [28, 32–34]. In particular, Critical Resolved Shear Stresses (CRSS) have been reported for at least four slip systems:  $[100](010)$ ,  $[001](010)$ ,  $[001](100)$ ,  $[001]\{110\}$ . Whereas the flow stress for dislocations with a  $[100]$  Burgers vector are only reported at high temperature, experiments performed to promote slip along  $[001]$  allow to plot the evolution of the CRSS as shown Figure 1, over a large range of temperatures. One may note that  $[001]\{110\}$  slip systems can be activated at low temperature [33] which even allowed a recent in-situ TEM deformation experiment [35] to activate in-situ glide of  $[001]$  dislocations in  $\{110\}$  at room temperature. The occurrence with  $[001]$  glide of a typical microstructure composed of long straight screw dislocation lines (e.g. [27] or [36]) suggests a relative high lattice friction on this character, whatever the glide plane. Recently, based on electron tomography, the three possible slip planes, i.e.  $(100)$ ,  $(010)$ , and  $\{110\}$ , have been reported simultaneously [37], but with a greater occurrence of  $\{110\}$ .

The last 15 years have also seen the development of different numerical methods to investigate the plastic properties of olivine. The earliest studies performed by Durinck and co-workers [38–40] relied on Density Functional Theory (DFT) calculations to compute Generalized Stacking Fault (GSF) energies [41] and to model dislocation core configurations using the Peierls Nabarro (PN) model [1, 3]. The PN model can provide some mechanical information through the computation of the Peierls stress, but has to be handled with care when dealing with complex crystal structures. Whereas the PN model gives satisfactory results in case of planar core configurations, it can also lead to several artifacts when the dislocation cores are non-planar or dissociated [5, 42]. At the same period, Walker and co-workers [43–45] used empirical potential models to compute dislocation core structures via atomistic simulations. However, due to the limitations in computational efficiency of the codes existing at that time, mechanical properties were not inferred from the atomic core structures. More recently, the empirical potential formulation used

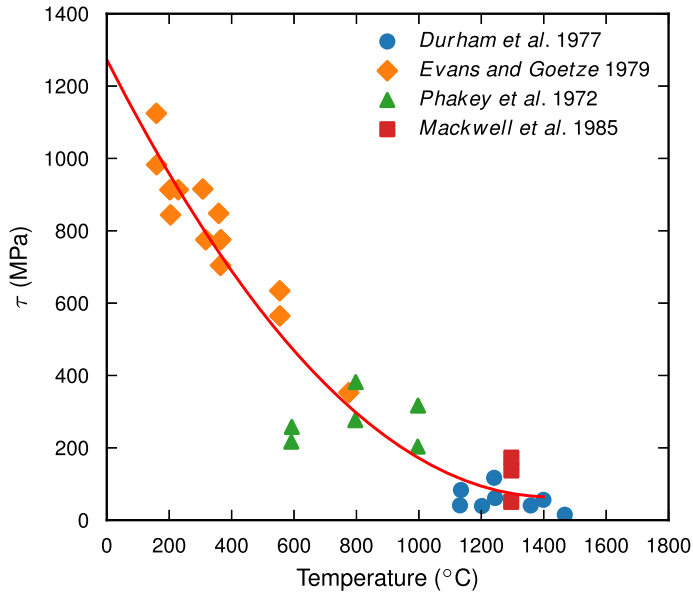


**Figure 1.** Summary of CRSS for [001] dislocations in olivine. Values are reported for the three slip systems [001](010) [28,34], [001](100) [32] and [001]{110} [33].

by Walker and co-workers was implemented into the molecular dynamics package LAMMPS [46] opening the route to revisit the dislocation core structure and properties in olivine [47]. As an example, in a recent study of Mahendran *et al.* [48], a detailed investigation of the structure of dislocations with a [100] Burgers vector highlighted the capabilities of [100] screw dislocations to cross-slip in various planes resulting in a pencil glide mechanism as invoked by Raleigh in olivine [26]. Up to now, in case of dislocations with a [001] Burgers vector, only one compact core structure of the screw dislocation has been reported [43,45,47].

In this study, we revisit the theoretical modeling of dislocation cores of [001] dislocations using quadrupolar arrangements of screw dislocations inserted in a periodic atomic system. As shown in the following section, the choice of a periodic system allows to compute accurately the dislocation core structure and its core energy. Finally, we show that our calculations allow to compute the lattice friction through the evaluation of the Peierls stress and account for high hydrostatic pressure effects, which are often debated in the field of mineral physics [49].

## 2. Methods

All calculations rely on the THB1 potential [50, 51] specifically derived to model  $\text{Mg}_2\text{SiO}_4$  forsterite, the Mg-rich end member of the olivine solid solution. In order to account for polarization effects in the material, the potential is parameterized with the inclusion of a core-shell (C/S) description of oxygen ions. The transferability of this potential parameterization has been checked in several studies [51], including calculations of GSF energies [47] which showed a rather good agreement with *ab initio* predictions [39]. With the THB1 parameterization, the lattice vectors of forsterite are  $a = 4.7874 \text{ \AA}$ ,  $b = 10.2717 \text{ \AA}$  and  $c = 6.0227 \text{ \AA}$ .

The core structure of [001] screw dislocations is computed using a fully periodic quadrupolar arrangement of dislocations. For ionic materials like forsterite, it is sometimes undesirable to have free surfaces, which can be charged and introduce artifacts or unquantified size effects [52]. Hence, a periodic system is preferred here to model dislocations and their properties.

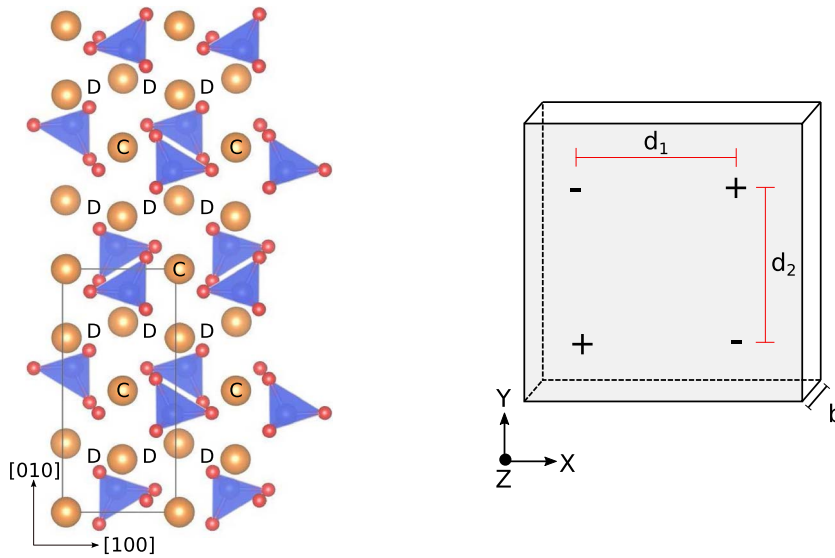


**Figure 2.** (left panel) View of the olivine crystal along  $[001]$  axis corresponding to the Burgers vector of the screw dislocations investigated in this study. Labels C and D corresponds to the initial centering of the dislocation elastic displacement field. (right panel) Quadrupolar arrangement of screw dislocations. As described in the Methods section,  $X$  and  $Y$  are respectively aligned with  $[100]$  and  $[010]$ .  $d_1$  and  $d_2$  refer to the periodic spacing between opposite dislocation lines.

Periodic arrays of dislocations include size effects, however they can be fully quantified and corrected [53]. The quadrupolar system is created by introducing four screw dislocations with two positive and two negative Burgers vectors in a  $\text{Mg}_2\text{SiO}_4$  crystal oriented along  $X = [100]$ ,  $Y = [010]$  and  $Z = [001]$  as shown in Figure 2. The inherent size effect, mostly resulting from the distances between dislocations, is carefully monitored by increasing the bulk dimension along the  $X$  and  $Y$  directions, leading to systems containing between 5632 atoms and 35,200 atoms. The alternate arrangement of dislocations with opposite Burgers vectors helps to reduce the long-range elastic fields of the four dislocations [53, 54]. Practically, the screw dislocations are introduced into the system thanks to the classical displacement field relying either on isotropic elasticity solutions, or on anisotropic elasticity as implemented in the AtomsK software [55]. The core structures of dislocations are analyzed after a minimization of the total energy and atomic forces as determined by the classical conjugate gradient algorithm implemented in the LAMMPS package. Relying on an empirical potential involving long range Coulombic interaction, it is worth noticing that the long range energy is computed thanks to Wolf summation methods [56] with a cut-off radius of 16 Å.

In this study, the lattice friction is quantified through the evaluation of the Peierls stress computed by a quasi-static loading of the simulation cell (e.g. [57]). As an example, to trigger the motion of a screw dislocation, here aligned with the  $Z$ -direction, in a glide plane normal to the  $Y$ -direction, the system is statically loaded with a shear strain increment  $\epsilon_{yz}$  (typically 1%). After each increment, the system is relaxed. As a result, the stress in the system increases linearly and the stress-strain curves deviate from linearity for a critical stress at which one can check that the dislocation starts to move, defining the onset of the plastic regime, i.e. the Peierls stress. Again, to avoid spurious effects of periodic boundary conditions, such calculations are repeated with gradual increase in simulation cell sizes along  $X$ ,  $Y$  directions from 40 Å to 100 Å to ensure independence with the system size.

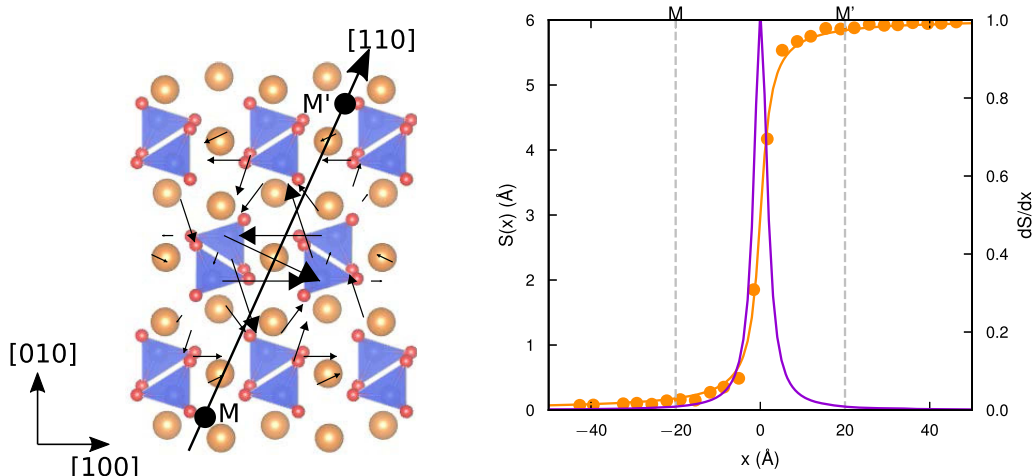


**Figure 3.** (left panel) Differential displacement map of the compact “C” dislocation core structure as calculated using 3D periodic boundary conditions. The arrows show the differential displacement between the neighbouring Si ions. The spreading of the dislocation core is found in agreement with those reported in [45]. (right panel) Disregistry function of [001] Burgers vector versus the position along the dislocation in  $(1\bar{1}0)$ . The disregistry function  $S$  along  $[110]$  shows a single density peak characteristic of a compact core configuration.

### 3. Results

Inserting a  $[001]$  dislocation into the olivine structure leads to two possible dislocation core configurations depending on the exact position of the initial dislocation center (Figure 2). The resulting core structures are labeled “C” and “D” according to the center position of the core.

#### 3.1. Compact versus dissociated core structure

A first core configuration named in the following “C” is obtained by centering the dislocation lines in the vicinity of the Mg cation site between four  $\text{SiO}_4$  tetrahedra (Figure 2). The analysis of the minimized atomic configurations reveals that all significant differential displacement between neighboring atoms are restricted to a small area within less than one unit cell around the dislocation line (Figure 3). Thus, the core appears to be compact with no particular evidence of spreading in any preferential plane. Such a compact core configuration is consistent with previous attempts to model screw dislocation cores in forsterite using THB1 potential [43,45,47], although the geometry of the simulated volumes is here different. Indeed, compared to the fully periodic system used here, all previous atomistic simulations were performed using either a “cluster” approach with fixed boundary shells of cylindrical symmetry around the dislocation line [43,45], or with semi-periodic boundary conditions and free surfaces [47].

However, we find a second core configuration, labeled “D”, by inserting a  $[001]$  dislocation line in the  $(010)$  plane containing Mg cations between  $\text{SiO}_4$  tetrahedra layers (Figure 2). After relaxation of the atomic positions to ensure the minimization of the total energy of the system, the relaxed screw dislocation core exhibits a clear spreading in one of the  $\{110\}$  planes as shown by the differential displacement map (Figure 4). Further details on the core structure are revealed by the disregistry analysis ( $S(x)$ ) in the cationic sub-lattice and its first derivative in the  $[110]$  plane (Figure 4). The dislocation core structure “D” corresponds to a core dissociated into a set of

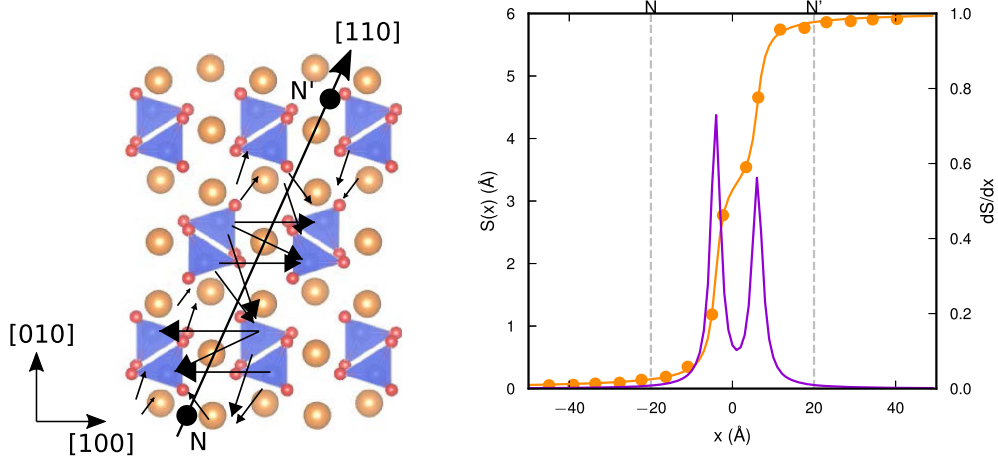


**Figure 4.** (left panel) Differential displacement map of the dissociated “D” dislocation core structure. Such a dissociated core configuration is obtained after inserting the dislocation elastic field centered on D position as shown in Figure 2. (right panel) The corresponding disregistry function along [110] in (110) highlights the dissociation into two partial dislocations.

two partial dislocations of almost equal partial Burgers vector  $b_p$ . The derivative of the disregistry function  $dS/dx$  highlights the dissociation with two isolated peaks of Burgers vector density (with similar half-width between 1.4 and 1.5 Å) separated by a distance of  $R = 10.2$  Å. As no evidence of edge displacement components is detected around the dislocation core, one can conclude that the dissociation into partial dislocations is fully collinear. In the following, we thus assume that the two partial dislocations have the same Burgers vector  $b_p = 1/2[001]$ . Such a dissociation is consistent with the existence of a stable stacking fault in {110} plane [40] as further discussed in Section 4.

### 3.2. Dislocation core energy

For both types of dislocation cores, “C” and “D” described above, the energies of minimized quadrupole systems were computed by varying the simulation box dimensions (hereafter called  $d_1$  and  $d_2$  and shown in Figure 1) from 75 Å to 200 Å along the  $X$  and  $Y$  directions. These calculations were performed to identify the core configuration with the lowest energy. Indeed, for screw dislocations arranged in a quadrupole system, the energy  $E$  of the dislocation core per unit Burgers vector length  $b$  scales with the intrinsic lengths ( $d_1, d_2$ ) of the dislocation arrangement according to the following relationship [58]:

$$E = E_{\text{core}} + E_{\text{elast}} = E_{\text{core}} + \frac{\mu b^3}{4\pi} (\ln(d_1/r_c) + A(d_1/d_2)). \quad (1)$$

In (1),  $E$  corresponds to the energy difference between a system containing a quadrupole of dislocations and a defect free crystal. The dislocation energy can then be decomposed into a core energy  $E_{\text{core}}$  and an elastic energy  $E_{\text{elast}}$  resulting from the periodic interactions between the dislocations in the system. In the elastic energy expression,  $d_1$  and  $d_2$  are the distances between the positive and negative dislocations (or the reduce scales of the system along  $X$  and  $Y$  directions respectively),  $A$  is a constant characteristic of the reduce scales ( $d_1/d_2$ ),  $\mu$  is the anisotropic shear modulus and  $r_c$  is a cut-off radius for the core energy.



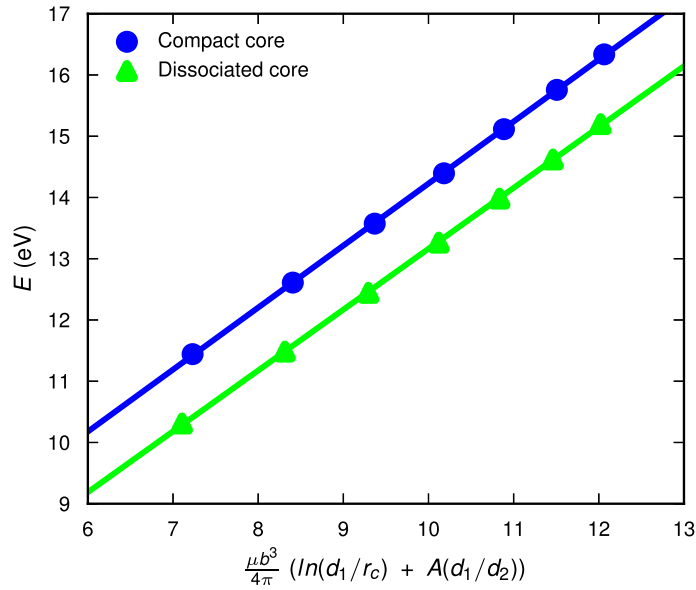


**Figure 5.** Dislocation core energy as a function of elastic energy stored in the quadrupole configuration. The screw dislocation core dissociated into collinear partial dislocations in  $\{110\}$  are of lowest energy.

Figure 5 shows the evolution of the dislocation energy for the two types of dislocations as a function of the elastic energy stored in the system. For both configurations, the energies increase linearly with the elastic energy (as defined in the previous equation). Moreover, as the difference between the two dislocation configurations are restricted to the core configuration, the elastic field should be identical as confirmed here by the similar slopes of the data point in Figure 5. For both dislocation cores, the elastic interaction energy scales with a shear modulus  $\mu = 48.6$  GPa, which is comparable with the isotropic shear modulus (65 GPa) estimated from the elastic moduli [47]. Whatever the system size, the energy of the dissociated configuration “D” is lower than those of the compact configuration, meaning that the dissociated core is to the stable core configuration. One may note that the dislocation core energies for core configurations of types “C” and “D” are noticeably different with 4.1036 eV/b (0.6813 eV/Å) and 3.2251 eV/b (0.5355 eV/Å) respectively.

As in the Earth mantle, olivine is found at depths where pressure may reach more than 10 GPa, we checked the stability of these two configurations by rescaling the computed volume to a given pressure. We then verified that up to 10 GPa, the dissociated core configuration is the most stable configuration for the screw dislocation core with no noticeable effect on the dissociation width (Table 1).

### 3.3. Lattice friction evaluation

Earlier studies [45, 47] suggested the possibility of a locking–unlocking mechanism [59] associated with the glide of  $[001]$  dislocations in  $(010)$  or in  $(100)$ . However, this was assumed based on the behavior of what we call here the compact “C” screw dislocation core. In order to check the validity of this assumption, we used similar quasi-static loading simulations to investigate the lattice friction associated with the stable dissociated dislocation core “D” found here.

**Table 1.** Characteristics of [001] dissociated dislocations

Pressure (GPa)	$R$ (Å)	$\sigma_{(1\bar{1}0)}$ (GPa)	$\sigma_{(010)}$ (GPa)
0	10.19	1.51	6.10
4	10.44	1.63	6.04
6	10.54	1.6	5.82
10	8.94	1.6	5.32

$R$  corresponds to the width between partial dislocations.  $\sigma_{(1\bar{1}0)}$  and  $\sigma_{(010)}$  correspond respectively to the critical stress at which the dislocation glides in  $(1\bar{1}0)$  or unlocks in order to glide in  $(010)$ .

Therefore, we incrementally increased the applied strain increment  $\epsilon_{yz}$  on our periodic system containing “D” dislocations, to promote glide in  $(010)$ . Up to a strain corresponding to a stress of 6.10 GPa, the system behaves elastically. At or above the critical stress, an analysis of the conjugate gradient minimizer steps shows that once the four dislocations are set (simultaneously) into motion, all the dislocations exhibit a different core structure, entirely planar, spread in  $(010)$ , identical to the one computed using the PN model in Ref. [45]. Moreover, as described in Ref. [47], such a planar configuration cannot be stabilized without applying strain (or stress) to the simulation cell and once this transient planar state is reached, the dislocation core can travel over several lattice repeats before finally falling back into another stable dissociated core configuration.

Using the same methodology, we applied a quasi-static loading process with a simple shear  $\epsilon_{xz}$  to promote glide in  $(100)$ . In this case, we observe that the dissociated core starts to glide in  $\{110\}$  at an applied stress of 3.9 GPa corresponding to a resolved shear stress of 1.5 GPa in the  $\{110\}$  glide plane. As the dislocation glides in  $\{110\}$ , we observed a continuous displacement of both partial dislocations so that the stacking fault remained constant.

#### 4. Discussion

Our calculations show that the stable configuration of [001] screw dislocations corresponds to a dislocation core dissociated in  $\{110\}$ . The dissociation width between partials is proportional to the energy ( $\gamma$ ) of the  $1/2[001]\{110\}$  stacking fault. For a separation distance  $R$ , the stacking fault energy between two partial screw dislocations (with Burgers vectors  $b_p = 1/2[001]$ ) can be estimated with the following elastic equilibrium equation [2].

$$\gamma = \frac{\mu b_p^2}{2\pi R}. \quad (2)$$

For the minimized dissociation distance of  $R = 10.2$  Å, the stacking fault energy is  $0.0457$  eV/Å<sup>2</sup>. On the other hand, from the calculation of the  $[001]\{110\}$  GSF [47] performed by constraining the Si atoms to move perpendicular to the glide plane while Mg and O atoms are allowed to freely relax in all directions, the  $\gamma$  energy associated with the  $1/2[001]\{110\}$  fault is  $0.042$  eV/Å<sup>2</sup>. The good agreement between the energies of the stacking fault, derived from the GSF calculations or the core configuration is noticeable. This not only emphasizes that the stacking fault configuration within the dislocation core should be close to the atomic configuration modeled in GSF calculations. But also, since a similar stable stacking fault is also computed by DFT calculations [40], one can argue that the same scheme of dissociation should be expected in DFT calculations and that our dissociated dislocation core is not potential parameterization dependent.

Regarding the effect of high pressure on the core structure, we note that the width between partial dislocations is almost pressure insensitive (Table 1). This trend is fully consistent with

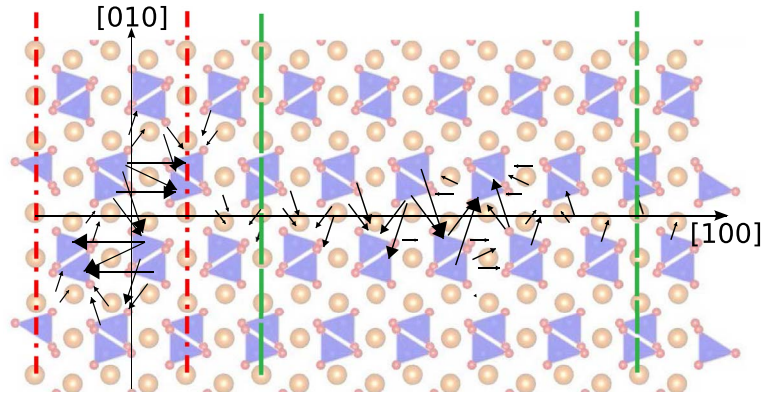


**Figure 6.** Schematic representation of unlocking mechanism of [001] dislocation. The stable dissociated core (at the left) when quasi-statically loaded beyond the critical stress value transforms into a high energy planar core (on the right) spread in (010) to unlock itself.

Durinck *et al.* results [39] for [001](110) stacking fault energies calculated using DFT simulations showing that for the same pressure range, the GSF energy corresponding to  $1/2[001]\{110\}$  remains rather constant.

Earlier studies [45, 47] suggested the possibility of a locking–unlocking mechanism associated with the glide of [001] dislocations in (010). However, this was assumed based on the behavior of what we call here the compact “C” screw dislocation core, which is not the most stable configuration. Thus, we have re-investigated the glide mechanisms starting from the stable dissociated core “D”. We show that when it is forced to glide in (010), the “D” screw dislocation core also transforms into a transient planar core in (010) (Figure 6). The critical stress at which the dislocation transforms into the transient planar configuration is found here 20% higher than the previously reported value for the compact core. This can be, at least qualitatively, attributed to the difference of core energy; the most stable core configuration with the lowest core energy requiring a larger stress to evolve into the transient state. Overall, we confirm that the activation of [001](010) slip system in olivine should exhibit a jerky motion of screw dislocations accordingly to a locking–unlocking mechanism [59].

Qualitatively our calculations are in agreement with experimental observations of dislocation dynamics at low pressure. Recently, using in situ TEM nanomechanical testing at ambient temperature, Idrissi and co-workers [35] observed the glide of [001] dislocations in {110}. At the scale of the observation (timescale corresponding to the video capture, and length-scale corresponding to the spatial resolution in weak-beam dark-field) glide was observed to be smooth. This behavior is in agreement with the planar configuration of the dislocation core that we propose although the dissociation width of a few tens of Angstroms cannot be distinguished by conventional TEM. Quantitatively, our results show that [001] dislocation glide in {110} at low temperature (as our calculations are performed using molecular statics) can be activated with a Peierls stress value of 1.51 GPa. This value is slightly larger than the stress measured at ambient temperature by Idrissi but compares well within the range of CRSS values in intermediate temperature range obtained experimentally (Figure 1).

In order to build a model of crystalline plasticity, one has to describe the collective response of dislocations within a given microstructure. Nowadays, the collective behavior of dislocations can be accurately treated by several mesoscale simulations called Dislocation Dynamics (DD) [60]. One of the most critical input of DD simulations is the mobility law of dislocations. This depends

critically on the dislocation core structure that one can determine from atomistic calculations, but also from the knowledge of the glide mechanism. In case of glide governed by the kink pairs mechanism, the mobility of dislocations at finite temperature can be inferred by atomistic simulations which account for the nucleation enthalpy and migration barriers of kinks [12, 23, 61]. For the peculiar case of [001] dislocations in olivine, whatever the glide plane, several issues arise. In order to properly define a velocity, one has to model kink nucleation and migration of dissociated dislocations or the atomic mechanism responsible for the strong core modifications involved into the locking–unlocking mechanism. For the latter mechanism, one has first to elucidate the atomistic mechanism alloying the transformation into a transient core. Such a mechanism should involve atomic configurations of macro-kinks for which the height is unconstrained and depends on the jump distance. As pointed out in Ref. [59], the probability of unlocking events should be length-dependent whereas the dislocation velocity is not. According to this scheme, finite length calculations with a detailed inspection of the energy landscape will be mandatory. This is out of the scope of the present study and is left for future work.

## 5. Conclusion

In this study, we characterized the stable configuration for the screw dislocations of [001] Burgers vector in olivine  $\text{Mg}_2\text{SiO}_4$ . Compared to the compact non-planar core proposed in previous studies, we demonstrate here that a dissociated core with two  $1/2[001]$  partial dislocations separated in a  $\{110\}$  plane corresponds to the stable configuration of the screw dislocation in olivine. This stable core of type “D” was subjected to gradual shear loading to extract information on lattice friction in different slip systems. We confirm that the glide of [001] screw dislocation in a (010) plane requires a core transformation here reached at stress values greater than 6 GPa. Such a transformation into a planar transient core can be interpreted as the signature at the atomic scale of a locking–unlocking mechanism. On the contrary, glide in  $\{110\}$  exhibits a smooth behavior and glide for applied resolved shear stress below 1.5 GPa.

## Acknowledgements

This work was supported by funding from the European Research Council under the Seventh Framework Programme (FP7), ERC Grant No 290424 – RheoMan, and under the Horizon 2020 research and innovation programme ERC Grant No 787198 – TimeMan. Computational resources were provided by the DSI-Universite de Lille.

## References

- [1] R. Peierls, “The size of a dislocation”, *Proc. Phys. Soc.* **52** (1940), p. 34-37.
- [2] J. Hirth, J. Lothe, *Theory of Dislocations*, Wiley, New York, 1982.
- [3] F. Nabarro, “Dislocations in a simple cubic lattice”, *Proc. Phys. Soc.* **59** (1947), p. 256-272.
- [4] J. Hartford, B. von Sydow, G. Wahnström, B. Lundqvist, “Peierls barriers and stresses for edge dislocations in Pd and Al calculated from first principles”, *Phys. Rev. B* **58** (1998), p. 2487-2495.
- [5] G. Schoeck, “The core structure of dislocations: Peierls model vs. atomic simulation”, *Acta Mater.* **54** (2006), no. 18, p. 4865-4870.
- [6] D. Rodney, L. Ventelon, E. Clouet, L. Pizzagalli, F. Willaime, “Ab initio modeling of dislocation core properties in metals and semiconductors”, *Acta Mater.* **124** (2017), p. 633-659.
- [7] T. Vegge, K. W. Jacobsen, “Atomistic simulations of dislocation processes in copper”, *J. Phys. Condens. Matter.* **14** (2002), no. 11, p. 2929-2956.
- [8] V. Vitek, V. Paidar, “Chapter 87 Non-planar dislocation cores: a ubiquitous phenomenon affecting mechanical properties of crystalline materials”, in *Dislocations in Solids* (J. Hirth, ed.), vol. 14, Elsevier, Amsterdam, 2008, p. 440-514.

- [9] R. Gröger, A. G. Bailey, V. Vitek, "Multiscale modeling of plastic deformation of molybdenum and tungsten: I. Atomistic studies of the core structure and glide of  $1/2\langle 111 \rangle$  screw dislocations at 0 K", *Acta Mater.* **56** (2008), p. 5401-5411.
- [10] N. Chaari, E. Clouet, D. Rodney, "First-principles study of secondary slip in zirconium", *Phys. Rev. Lett.* **112** (2014), article no. 075504 (5 pages).
- [11] W. Xu, J. Moriarty, "Accurate atomistic simulations of the Peierls barrier and kink-pair formation energy for  $\langle 111 \rangle$  screw dislocations in bcc Mo", *Comput. Mater. Sci.* **9** (1998), p. 348-356.
- [12] L. Provaille, D. Rodney, M.-C. Marinica, "Quantum effect on thermally activated glide of dislocations", *Nat. Mater.* **11** (2012), p. 845-849.
- [13] L. Pizzagalli, A. Pedersen, A. Arnaldsson, H. Jónsson, P. Beauchamp, "Theoretical study of kinks on screw dislocation in silicon", *Phys. Rev. B* **77** (2008), article no. 064106.
- [14] T. T. Lau, X. Lin, S. Yip, K. J. V. Vliet, "Atomistic examination of the unit processes and vacancy-dislocation interaction in dislocation climb", *Scr. Mater.* **60** (2009), p. 399-402.
- [15] M. Landeiro Dos Reis, L. Provaille, M. Sauzay, "Modeling the climb-assisted glide of edge dislocations through a random distribution of nanosized vacancy clusters", *Phys. Rev. Mater.* **2** (2018), article no. 093604.
- [16] J.-H. Zhai, P. Hirel, P. Carrez, "Atomic-scale properties of jogs along  $1/2\langle 110 \rangle$  edge dislocations in MgO", *Scr. Mater.* **181** (2020), p. 66-69.
- [17] R. Pasianot, D. Farkas, E. J. Savino, "Dislocation core structure in ordered intermetallic alloys", *J. Phys. III France* **1** (1991), p. 997-1014.
- [18] M. Puls, C. So, "The core structure of an edge dislocation in NaCl", *Phys. Status Solidi* **98** (1980), p. 87-96.
- [19] G. Watson, E. Kelsey, S. Parker, "Atomistic simulation of screw dislocations in rock salt structured materials", *Phil. Mag. A* **79** (1999), p. 527-536.
- [20] A. M. Walker, B. Slater, J. D. Gale, K. Wright, "Predicting the structure of screw dislocations in nanoporous materials", *Nat. Mater.* **3** (2004), p. 715-720.
- [21] P. Carrez, D. Ferre, P. Cordier, "Implications for plastic flow in the deep mantle from modelling dislocations in MgSiO<sub>3</sub> minerals", *Nature* **446** (2007), p. 68-70.
- [22] P. Hirel, M. Mrovec, C. Elsässer, "Atomistic study of  $\langle 110 \rangle$  dislocations in strontium titanate", *Acta Mater.* **60** (2012), p. 329-338.
- [23] A. Kraych, P. Carrez, P. Hirel, E. Clouet, P. Cordier, "Peierls potential and kink-pair mechanism in high-pressure MgSiO<sub>3</sub> perovskite: An atomic scale study", *Phys. Rev. B* **93** (2016), article no. 014103.
- [24] J. R. Smyth, R. M. Hazen, "The crystal structures of forsterite and hortonolite at several temperatures up to 900 °C", *Am. Mineral.* **58** (1973), p. 588-593.
- [25] D. J. Barber, H.-R. Wenk, G. Hirth, D. L. Kohlstedt, "Chapter 95 dislocations in minerals", in *Dislocations in Solids* (J. Hirth, ed.), vol. 16, Elsevier, Amsterdam, 2010, p. 171-232.
- [26] C. B. Raleigh, "Mechanisms of plastic deformation of olivine", *J. Geophys. Res.* **73** (1968), p. 5391-5406.
- [27] D. L. Kohlstedt, C. Goetze, W. B. Durham, J. V. Sande, "New technique for decorating dislocations in olivine", *Science* **191** (1976), p. 1045-1046.
- [28] W. B. Durham, C. Goetze, "Plastic flow of oriented single crystals of olivine: 1. Mechanical data", *J. Geophys. Res.* **82** (1977), p. 5737-5753.
- [29] M. Darot, Y. Gueguen, "High-temperature creep of forsterite single crystals", *J. Geophys. Res.* **86** (1981), p. 6129-6234.
- [30] Y. Gueguen, "Dislocations in naturally deformed terrestrial olivine: classification, interpretation, applications", *Bull. Mineral.* **102** (1979), p. 178-183.
- [31] N. L. Carter, H. G. Ave'Lallemant, "High temperature flow of dunite and peridotite", *Geol. Soc. Am. Bull.* **81** (1970), p. 2181-2202.
- [32] P. Phakey, G. Dollinger, J. Christie, "Transmission electron microscopy of experimentally deformed olivine crystals", in *Flow and Fracture of Rocks*, American Geophysical Union (AGU), Washington, DC, 1972, p. 117-138.
- [33] B. Evans, C. Goetze, "The temperature variation of hardness of olivine and its implication for polycrystalline yield stress", *J. Geophys. Res.* **84** (1979), p. 5505-5524.
- [34] S. J. Mackwell, D. L. Kohlstedt, M. S. Paterson, "The role of water in the deformation of olivine single crystals", *J. Geophys. Res.* **90** (1985), article no. 11319.
- [35] H. Idrissi, C. Bollinger, F. Boioli, D. Schryvers, P. Cordier, "Low-temperature plasticity of olivine revisited with in situ TEM nanomechanical testing", *Sci. Adv.* **2** (2016), article no. e1501671.
- [36] R. J. Gaboriaud, M. Darot, Y. Gueguen, J. Woignard, "Dislocations in olivine indented at low temperatures", *Phys. Chem. Miner.* **7** (1981), p. 100-104.
- [37] A. Mussi, P. Cordier, S. Demouchy, C. Vanmansart, "Characterization of the glide planes of the  $\{001\}$  screw dislocations in olivine using electron tomography", *Phys. Chem. Miner.* **41** (2014), p. 537-545.
- [38] J. Durinck, A. Legris, P. Cordier, "Influence of crystal chemistry on ideal plastic shear anisotropy in forsterite: First principle calculations", *Am. Mineral.* **90** (2005), p. 1072-1077.

- [39] J. Durinck, A. Legris, P. Cordier, "Pressure sensitivity of olivine slip systems: First-principle calculations of generalised stacking faults", *Phys. Chem. Miner.* **32** (2005), p. 646-654.
- [40] J. Durinck, P. Carrez, P. Cordier, "Application of the Peierls-Nabarro model to dislocations in forsterite", *Eur. J. Mineral.* **19** (2007), p. 631-639.
- [41] V. Vitek, "Intrinsic stacking faults in body-centred cubic crystals", *Phil. Mag.* **18** (1968), p. 773-786.
- [42] G. Schoeck, "The Peierls model: Progress and limitations", *Mater. Sci. Eng. A* **400-401** (2005), p. 7-17.
- [43] A. M. Walker, J. D. Gale, B. Slater, K. Wright, "Atomic scale modelling of the cores of dislocations in complex materials part 1: methodology", *Phys. Chem. Chem. Phys.* **7** (2005), p. 3227-3234.
- [44] A. M. Walker, J. D. Gale, B. Slater, K. Wright, "Atomic scale modelling of the cores of dislocations in complex materials part 2: applications", *Phys. Chem. Chem. Phys.* **7** (2005), p. 3235-3242.
- [45] P. Carrez, A. Walker, A. Metsue, P. Cordier, "Evidence from numerical modelling for 3D spreading of [001] screw dislocations in Mg<sub>2</sub>SiO<sub>4</sub> forsterite", *Phil. Mag.* **88** (2008), p. 2477-2485.
- [46] S. Plimpton, "Fast parallel algorithms for short-range molecular dynamics", *J. Comput. Phys.* **117** (1995), p. 1-19.
- [47] S. Mahendran, P. Carrez, S. Groh, P. Cordier, "Dislocation modelling in Mg<sub>2</sub>SiO<sub>4</sub> forsterite: an atomic-scale study based on the THB1 potential", *Modell. Simul. Mater. Sci. Eng.* **25** (2017), article no. 054002.
- [48] S. Mahendran, P. Carrez, P. Cordier, "On the glide of [100] dislocation and the origin of 'pencil glide' in Mg<sub>2</sub>SiO<sub>4</sub> olivine", *Phil. Mag.* **99** (2019), p. 2751-2769.
- [49] D. Mainprice, A. Tommasi, H. Couvy, P. Cordier, D. J. Frost, "Pressure sensitivity of olivine slip systems and seismic anisotropy of Earth's upper mantle", *Nature* **433** (2005), p. 731-733.
- [50] G. D. Price, S. C. Parker, "Computer simulations of the structural and physical properties of the olivine and spinel polymorphs of Mg<sub>2</sub>SiO<sub>4</sub>", *Phys. Chem. Miner.* **10** (1984), p. 209-216.
- [51] G. D. Price, S. C. Parker, "The lattice dynamics of forsterite", *Min. Mag.* **51** (1987), no. 359, p. 157-170.
- [52] A. M. Walker, P. Carrez, P. Cordier, "Atomic-scale models of dislocation cores in minerals: progress and prospects", *Min. Mag.* **74** (2010), p. 381-413.
- [53] N. Lehto, S. Öberg, "Effects of dislocation interactions: Application to the period-doubled core of the 90° partial in silicon", *Phys. Rev. Lett.* **80** (1998), p. 5568-5571.
- [54] W. Cai, V. V. Bulatov, J. Chang, J. Li, S. Yip, "Periodic image effects in dislocation modelling", *Phil. Mag.* **83** (2003), p. 539-567.
- [55] P. Hirel, "Atomsk: A tool for manipulating and converting atomic data files", *Comput. Phys. Commun.* **197** (2015), p. 212-219.
- [56] D. Wolf, P. Keblinski, S. R. Phillpot, J. Eggebrecht, "Exact method for the simulation of Coulombic systems by spherically truncated, pairwise  $r^{-1}$  summation", *J. Chem. Phys.* **110** (1999), no. 17, p. 8254-8282.
- [57] P. Hirel, A. Kraych, P. Carrez, P. Cordier, "Atomic core structure and mobility of [100](010 and [010](100) dislocations in MgSiO<sub>3</sub> perovskite", *Acta Mater.* **79** (2014), p. 117-125.
- [58] S. Ismail-Beigi, T. a. Arias, "Ab initio study of screw dislocations in Mo and Ta: A new picture of plasticity in bcc transition metals", *Phys. Rev. Lett.* **84** (2000), p. 1499-1502.
- [59] D. Caillard, J.-L. Martin, *Thermally Activated Mechanisms in Crystal Plasticity*, Pergamon Materials Series, vol. 8, Elsevier, Oxford, 2003.
- [60] L. Kubin, *Dislocations, Mesoscale Simulations and Plastic Flow*, Oxford Series on Materials Modelling, Oxford University Press, 2013.
- [61] J. Amodeo, P. Carrez, B. Devincere, P. Cordier, "Multiscale modelling of MgO plasticity", *Acta Mater.* **59** (2011), p. 2291-2301.